ARL-TR-10 AR-007-102

DEPARTMENT OF DEFENCE

DEFENCE SCIENCE AND TECHNOLOGY ORGANISATION

AERONAUTICAL RESEARCH LABORATORY

MELBOURNE, VICTORIA

Technical Report 10

COMPUTATION OF NON-ISENTROPIC INTERNAL FLOWS WITH VARIABLE DENSITY

by

E. BRIZUELA

Approved for public release

NOVEMBER 1993

AR-007-102

DEPARTMENT OF DEFENCE
DEFENCE SCIENCE AND TECHNOLOGY ORGANISATION
AERONAUTICAL RESEARCH LABORATORY

Technical Report 10

COMPUTATION OF NON-ISENTROPIC INTERNAL FLOWS WITH VARIABLE DENSITY

by

E. BRIZUELA

SUMMARY

A computational fluid dynamics code named MULTIFLOW-2D has been acquired and is being put into service for the numerical simulation of gas turbine-type combustors.

Certain areas of the code were found to be in need of improvement for this application; these are:

- *The grid generation algorithm*
- *The manner of discretisation of the continuity and momentum equations, and*
- *The treatment of the inlet boundary conditions.*

Improvements to these areas were developed and incorporated to the code, and the code functioning in non-reactive flows was tested by means of numerical experiments; verification against physical experiments is planned.

DSTO AUSTRALIA

POSTAL ADDRESS: Director, Aeronautical Research Laboratory
506 Lorimer Street, Fishermens Bend
Victoria 3207, Australia.

TABLE OF CONTENTS

1. INTRODUCTION

As part of a program to develop a capability in computational modeling of gas turbine combustor flows, the MULTIFLOW-2D code is being adapted for application to this purpose. The code was obtained from the Aero Propulsion and Power Directorate of the US Air Force Wright Laboratory under the Mutual Weapons Development Data Exchange Agreement Annex 7017.

The code has been modified both to correct deficiencies and to introduce features necessary for the intended application.

2. THE MULTIFLOW-2D CODE

2.1 Brief description

The theoretical basis of this code is detailed by its author in Refs [1] and [2], while further description of the code capabilities and general features may be found in [3].

In brief, the code finds solutions to the conservation equations of flow discretised in finite volume form. The discretisation points form a grid which covers the flow region using an equal number of points per grid line (Boundary Fitted Coordinate system). The flow may be two-dimensional or axisymmetric (including axisymmetric rotation, termed swirl).

Solutions are found for the conservation of mass, linear momentum, energy and chemical species. Closure of the conservation equations for turbulent flows is obtained by means of the two-equation $\kappa - \epsilon$ model; the stochastic turbulent diffusion flame model uses an assumed probability distribution function generated using its first two moments (mean and rms), which are obtained from their own transport equations. There is also a facility to simulate liquid fuel sprays.

The solution process includes a multigrid system, whereby coarse grids are utilised to remove the low frequency errors which slow down the convergence of the fine grids.

2.2 Improvements required

The code was installed in the local computer system, "debugged" and tested until qualitatively satisfactory computations were obtained for a number of cases including that of an annular jet discharging into a sudden expansion (with and without a coflowing centre jet) and a separating diffuser. However, the operation of certain code functions was deemed unsatisfactory, namely:

- Great difficulty/inability to use fine meshes, and
- Great difficulty/inability to compute flows with variable density.

Having achieved a degree of confidence in the operation of the code development work was initiated to overcome the observed difficulties. Section 3 of this Report describes the additions and modifications introduced to this effect. Difficulties in using very fine meshes were attributed to the manner in which coarse grids were generated from the finest grid, which is discussed in Section 3.1, and to the manner in which the coefficients of the discretised

equations were generated, which is discussed in Section 3.3.2. Difficulties in the computation of flows with variable density were attributed to the need for a more sophisticated discretisation of the continuity equation to take into account aero-thermodynamic relations, which is discussed in Section 3.2, and to the need to reformulate inlet boundary conditions to conserve total pressure, which is discussed in Section 3.3.1.

Validation of the new code against experimental results in non-reacting flows is planned for the near future. Section 4 presents examples of computational outputs to demonstrate the functioning of the code and some noteworthy features.

3. DEVELOPMENT OF MULTIFLOW-2D

3.1 Grid generation process

The difficulties experienced using very fine grids were investigated, and were attributed to the practice of generating fine grids by subdivision of coarse grids. This results in ill-fitting meshes, particularly about finite-radius corners, and is unsuitable for continuous curved boundaries, as shown in Fig 1. The grid generation algorithm was therefore turned about, to fit the finest mesh to the boundaries and obtain coarse meshes by skipping every second grid line, as illustrated in Fig 2. This allowed some examples to be computed to maximum grid fineness (6 grid levels), which was previously unachievable.

The revised scheme may introduce error in the process of changing from a coarse to a fine grid and *vice versa*. However, no error is introduced in the transformation of velocities on the basis of conservation of mass. Fig 3 shows that the projected areas dA are not affected by the fact that a coarse cell does not fully enclose four fine cells, because the extreme corners are common. It is still exact to say that, for instance:

$$(\rho U\, dA)^C_{i,j} = (\rho U\, dA)^F_{i,j} + (\rho U\, dA)^F_{i,j-1} \tag{1}$$

where ρ is density and U the component of velocity normal to A.

On the other hand, scalar quantities are transformed on the assumption that a fine cell is 1/4 the size of a coarse cell, and thence the centre of the coarse cell is the CG of the centres of the fine cells. Fig 3 shows that in the revised scheme an error may be introduced in that the point at which the coarse value is computed is C, where the coarse value of a scalar quantity S is given by:

$$S^C_{i,j} = \frac{1}{4}(S^F_{i,j} + S^F_{i-1,j} + S^F_{i,j-1} + S^F_{i-1,j-1}) \tag{2}$$

However, the coarse quantity $S^C_{i,j}$ should have been computed not at C but at the coarse cell centre $C^C_{i,j}$.

This added inaccuracy in the transfer of scalars between grids is of no consequence since in the Multigrid system used in MULTIFLOW-2D the finest grid (the reported solution grid) must in the end be converged on its own. Simple and relatively inaccurate transfer mechanisms between grids have no effect on the end result on the finest grid.

3.2 Discretisation of the Continuity equation

In the original formulation of MULTIFLOW-2D the continuity equation was discretised as for constant-density flow. For use in combustion it is necessary to be able to compute flows with large density variations, and where density is linked to temperature and pressure according to the laws of aero-thermodynamics.

Two areas require development in this respect: evaluation of the density-velocity product at a cell face, and compliance with the second law of thermodynamics.

3.2.1 Density interpolation

The mass flow rate across a cell face dA may be expressed as:

$$\rho U \, dA \, . \tag{3}$$

In the staggered-grid system presently used all scalar quantities (e.g., pressure and density) are computed at the cell centre. A cell is identified by its i, j indices and the coordinates of the top right-hand corner. Vectorial quantities U and V are computed at the centre of the cell faces adjacent to the identifying corner (Fig 4). It thence becomes necessary to interpolate density to obtain its value at the two cell faces for U and V. The challenge is to find an interpolation algorithm which is computationally inexpensive and has a basis in the physics of the problem.

One possible solution is standard spline fitting, in itself a computationally expensive process. Moreover, this requires four data points straddling each cell face, which leads to a computational stencil of at least 9 cells (Fig 5). This gives rise to a number of special cases near boundaries, a situation to be avoided as it is also computationally expensive.

At the other extreme the simple arithmetic average between adjacent cell centres may be adopted. This is computationally inexpensive and only requires the minimal 5-cell stencil. On the other hand, no information is transmitted regarding the physics of the problem, i.e., upstream and downstream values and gradients have the same weight.

An alternative has been given by Karki and Patankar [4], who adopt an upwinding approach, illustrated in Fig 6 for the west face. Calling

$$M(\phi) = \text{Largest of } \phi \text{ and } 0 \, , \tag{4}$$

then their interpolated value is:

$$\rho_w = \rho_W \frac{M(U_w)}{U_w} + \rho_P \frac{M(-U_w)}{U_w} \, . \tag{5}$$

As a result, density on the west face ρ_w will be the density at the west cell centre ρ_W if the flow is conventionally positive (West to East), and will be the density at the cell centre

ρ_P if the flow is from East to West. The underlying physical assumption is that density is primarily a convected property.

When coarse cells are utilised and combustion is expected it is desirable to retain some links to adjacent values. To this end the upwind concept has been extended to achieve a form which is as computationally simple as the last two above but still carries some higher level information. This is achieved by firstly considering an upwind-biased second order polynomial fit, i.e., with two data points upwind of the cell face and one downwind. This is exemplified in Fig 7 for the computation of density at the p face (the face corresponding with U_p).

Elementary algebra yields for a conventionally positive U:

$$\rho_p = \frac{1}{8}(3\rho_E + 6\rho_P - \rho_W)\,. \tag{6}$$

For U of the opposite sense:

$$\rho_p = \frac{1}{8}(3\rho_P + 6\rho_E - \rho_{EE})\,. \tag{7}$$

The switching function $M(U)$ may be used now to select one of the interpolating functions. With previous notation the interpolated values at the four faces, as used in Fig 8, are:

$$\rho_p = \frac{1}{8U_p}\left[(3\rho_E + 6\rho_P - \rho_W)M(U_p) + (3\rho_P + 6\rho_E - \rho_{EE})M(-U_p)\right](\text{at } U_p)\,, \tag{8}$$

$$\rho_w = \frac{1}{8U_w}\left[(3\rho_P + 6\rho_W - \rho_{WW})M(U_w) + (3\rho_W + 6\rho_P - \rho_E)M(-U_w)\right](\text{at } U_w)\,, \tag{9}$$

$$\rho_p = \frac{1}{8V_p}\left[(3\rho_N + 6\rho_P - \rho_S)M(V_p) + (3\rho_P + 6\rho_N - \rho_{NN})M(-V_p)\right](\text{at } V_p)\,, \tag{10}$$

$$\rho_s = \frac{1}{8V_s}\left[(3\rho_P + 6\rho_S - \rho_{SS})M(V_s) + (3\rho_S + 6\rho_P - \rho_N)M(-V_s)\right](\text{at } V_s)\,. \tag{11}$$

This is not as computationally expensive as the third-order spline fit but again it involves a 9-cell stencil (note cells EE, SS, NN, and WW).

A simplified algorithm is adopted instead, which may simply be described as:

$$\rho_{face} = \frac{1}{2}(\rho_{upwinded} + \rho_{averaged})\,. \tag{12}$$

For ρ_p at the U_p face and West to East flow the above expression yields:

$$\rho_p = \frac{1}{2}(\rho_P + \frac{\rho_P + \rho_E}{2})\,. \tag{13}$$

On the other hand the upwind-biased parabolic interpolation gives:

$$\rho_p = \frac{1}{8}(3\rho_E + 6\rho_P - \rho_W)\,. \tag{14}$$

The difference is:

$$\Delta\rho_p = \frac{1}{8}(\rho_E - \rho_W)\,. \tag{15}$$

This is almost an order of magnitude smaller than the *difference* in densities between upstream and downstream, i.e., the simplified algorithm (12) is a very close approximation to the upwind-biased parabolic fit.

It is seen that the simplified interpolation algorithm has the following properties:

- Computationally inexpensive (involves only the minimal stencil),
- Incorporates some upwind biasing in response to the physics of the problem, and
- Incorporates some higher level information, i.e., upwind slope.

3.2.2 Complying with the Second Law of Thermodynamics

Consider the computational cell P and adjacent locations shown in Fig 8.

The continuity equation may be written:

$$\rho U\,DU\,|_p - \rho U\,DU\,|_w - \rho V\,DV\,|_s + \rho V\,DV\,|_p = 0\,, \tag{16}$$

where DU,DV are the cell face areas normal to U,V. Densities are assumed interpolated as per the previous discussion.

The exact values of the variables are employed above, since the sum is equated to zero. Exact values can be related to current, approximate values (indicated by an asterisk) by means of corrections (indicated by primes):

$$\rho = \rho^* + \rho'\,, \tag{17}$$
$$U = U^* + U'\,, \tag{18}$$
$$V = V^* + V'\,. \tag{19}$$

Then, neglecting second-order products:

$$\rho U = \rho' U^* + \rho^* U' + \rho^* U^*\,, \tag{20}$$
$$\rho V = \rho' V^* + \rho^* V' + \rho^* V^*\,. \tag{21}$$

Substituting and rearranging:

$$\begin{aligned} &\rho^* U' \, DU \,|_p - \rho^* U' \, DU \,|_w - \rho^* V' \, DV \,|_s + \rho^* V' \, DV \,|_p \\ &+ \rho' U^* \, DU \,|_p - \rho' U^* \, DU \,|_w - \rho' V^* \, DV \,|_s + \rho' V^* \, DV \,|_p \;\; = \\ &- [\rho^* U^* \, DU \,|_p - \rho^* U^* \, DU \,|_w - \rho^* V^* \, DV \,|_s + \rho^* V^* \, DV \,|_p] \; . \end{aligned} \tag{22}$$

The right-hand side is the residual obtained when computing the continuity equation with all current values, which will be called RC.

The first four terms on the left-hand side involve current values of density and correction values for velocity. These are kept as they are and will be used to compute the four corrections U'_p, U'_w, V'_p, V'_s.

The next four terms are a challenge because they must be put in a form compatible with the discretised Navier-Stokes equations, i.e., in terms of velocity and pressure. The current values of velocity are left as they are, and the task is to express the density corrections ρ', which are placed at the U,V face locations, in terms of the pressure correction p'_P, which is located at the cell centre. This must be done in such a manner that the behaviour of the discretised equations is correct over the range of Mach numbers, changing from elliptic to hyperbolic as the flow changes from subsonic to supersonic.

The final form of the discretised continuity equation will be:

$$a_1 U'_w + a_2 U'_p + a_3 V'_s + a_4 V'_p + a_5 p'_P = F \; , \tag{23}$$

where:

$$a_1 = -\rho^* DU \,|_w \; , \tag{24}$$
$$a_2 = \rho^* DU \,|_p \; , \tag{25}$$
$$a_3 = -\rho^* DV \,|_s \; , \tag{26}$$
$$a_4 = \rho^* DV \,|_p \; , \tag{27}$$

and expressions must be found for a_5 and F.

The first step in linking ρ' and p' is to transform the four terms into expressions containing the cell-centred values by means of the interpolation formulae. The remaining four terms, i.e., the last four terms of Eq (22) were:

$$\rho' U^* \, DU \,|_p - \rho' U^* \, DU \,|_w - \rho' V^* \, DV \,|_s + \rho' V^* \, DV \,|_p \; . \tag{28}$$

Into this expression substitute the interpolated values of ρ' obtained using the interpolation procedure, i.e.:

$$\rho_p' = \frac{1}{2}\rho_P'\frac{M(U_p)}{U_p} + \frac{1}{2}\rho_E'\frac{M(-U_p)}{U_p} + \frac{1}{2}\frac{\rho_P' + \rho_E'}{2}(\text{at } U_p)\,, \tag{29}$$

$$\rho_w' = \frac{1}{2}\rho_W'\frac{M(U_w)}{U_w} + \frac{1}{2}\rho_P'\frac{M(-U_w)}{U_w} + \frac{1}{2}\frac{\rho_P' + \rho_W'}{2}(\text{at } U_w)\,, \tag{30}$$

$$\rho_p' = \frac{1}{2}\rho_P'\frac{M(V_p)}{V_p} + \frac{1}{2}\rho_N'\frac{M(-V_p)}{V_p} + \frac{1}{2}\frac{\rho_P' + \rho_N'}{2}(\text{at } V_p)\,, \tag{31}$$

$$\rho_s' = \frac{1}{2}\rho_S'\frac{M(V_s)}{V_s} + \frac{1}{2}\rho_P'\frac{M(-V_s)}{V_s} + \frac{1}{2}\frac{\rho_P' + \rho_S'}{2}(\text{at } V_s)\,. \tag{32}$$

(Asterisks have been conveniently dropped since only current values of velocity are involved)

Substituting Eqns (29)-(32) into (28) and rearranging:

$$\begin{aligned}
&\rho_P'(M(U_p) + \frac{U_p}{2})\frac{DU_p}{2} + \rho_E'(M(-U_p) + \frac{U_p}{2})\frac{DU_p}{2}\,,\\
&-\rho_W'(M(U_w) + \frac{U_w}{2})\frac{DU_w}{2} - \rho_P'(M(-U_w) + \frac{U_w}{2})\frac{DU_w}{2}\,,\\
&+\rho_P'(M(V_p) + \frac{V_p}{2})\frac{DV_p}{2} + \rho_N'(M(-V_p) + \frac{V_p}{2})\frac{DV_p}{2}\,,\\
&-\rho_S'(M(V_s) + \frac{V_s}{2})\frac{DV_s}{2} - \rho_P'(M(-V_s) + \frac{V_s}{2})\frac{DV_s}{2}\,.
\end{aligned} \tag{33}$$

Define and collect coefficients VA (for 'Velocity times Area'):

$$\text{Terms for } \rho_E' : VA_E = \ (M(-U_p) + \frac{U_p}{2})\frac{DU_p}{2}\,, \tag{34}$$

$$\text{Terms for } \rho_N' : VA_N = \ (M(-V_p) + \frac{V_p}{2})\frac{DV_p}{2}\,, \tag{35}$$

$$\text{Terms for } \rho_S' : VA_S = -(M(\ V_s) + \frac{V_s}{2})\frac{DV_s}{2}\,, \tag{36}$$

$$\text{Terms for } \rho_W' : VA_W = -(M(\ U_p) + \frac{U_p}{2})\frac{DU_p}{2}\,, \tag{37}$$

and for ρ_P':

$$VA_P = (M(U_p)+\frac{U_p}{2})\frac{DU_p}{2} - (M(-U_w)+\frac{U_w}{2})\frac{DU_w}{2} + (M(V_p)+\frac{V_p}{2})\frac{DV_p}{2} - (M(-V_s)+\frac{V_s}{2})\frac{DV_s}{2}\,. \tag{38}$$

The four terms (28) can now be expressed as five terms in cell-centred density corrections:

$$VA_P\rho_P' + VA_E\rho_E' + VA_N\rho_N' + VA_S\rho_S' + VA_W\rho_W' \ . \tag{39}$$

The next step is to relate the cell-centred density corrections to cell-centred pressure corrections. From the state equation:

$$\frac{d\rho}{\rho} = \frac{dp}{p} - \frac{dt}{t} \ , \tag{40}$$

and from the definition of entropy:

$$\frac{dt}{t} = \frac{ds}{C_p} + \frac{\gamma - 1}{\gamma}\frac{dp}{p} \ , \tag{41}$$

where s is entropy per unit mass in units of m^2/sec^2K, C_p is the specific heat at constant pressure and γ the adiabatic exponent.

Eliminating dt/t and using the definition of isentropic velocity of sound

$$c^2 = \gamma p/\rho \ , \tag{42}$$

results in:

$$d\rho = \frac{1}{c^2}(dp - \frac{\rho c^2}{C_p}ds) \ . \tag{43}$$

This equation can be put in Eulerian form as:

$$D\rho = \frac{1}{c^2}(Dp - \frac{\rho c^2}{C_p}Ds) \ . \tag{44}$$

Substituting the corrections for the differentials:

$$\rho' = \frac{1}{c^2}(p' - \frac{\rho c^2}{C_p}(Ds)') \ , \tag{45}$$

where $(Ds)'$ is a correction to the process entropy increase, arising from the corrections to velocities, densities, etc.

Call VH'(for 'Viscous Heating'):

$$VH' = \frac{\rho c^2}{C_p}(Ds)' \ , \tag{46}$$

and Eq (45) is written:

$$\rho' = \frac{1}{c^2}(p' - VH') \ . \tag{47}$$

In isentropic flow a pressure change p' produces a density change $\rho' = p'/c^2$. Viscosity raises the gas temperature, diminishing a density increase (if $p' > 0$) or reinforcing a density reduction (if $p' < 0$). Note that it is always $VH' \geq 0$.

Substituting ρ' the five terms (39) can be manipulated to yield:

$$\frac{VA}{c^2}p' \mid_P + \sum_{E,N,S,W}(\frac{VA}{c^2}p') - \sum_{P,E,N,S,W}(\frac{VA}{c^2}VH'). \tag{48}$$

This yields the desired coefficient of p'_P as:

$$a_5 = \frac{VA}{c^2} \mid_P \ . \tag{49}$$

Terms in the surrounding pressure corrections $\frac{VA}{c^2}p'$ are moved to the right-hand side, to be substracted from the continuity residual; thus, so far:

$$F \equiv RC - \sum_{E,N,S,W}(\frac{VA}{c^2}p') \ . \tag{50}$$

At this stage it is possible to consider the behaviour of the discretised equation. Neglecting residuals and entropy terms the continuity equation (from Eqns (23)-(27) and (49)) is of the form:

$$\rho U' \, DU + \frac{U \, DU}{c^2}p' \ . \tag{51}$$

This can be rearranged as:

$$\frac{DU}{U}(\rho UU' + M^2 p') \ . \tag{52}$$

The relative importance of the pressure and velocity corrections is seen to be proportional to the square of the Mach number. At low Mach numbers the velocity correction term will

predominate as is appropriate for elliptic flows, whereas at high Mach numbers the pressure term becomes dominant as is appropriate for hyperbolic flows.

There remains to express VH' in terms of velocity and pressure corrections. This is done by means of the energy equation taken in the following form [5]:

$$\rho\frac{Ds}{D\tau} = \frac{\Phi}{t} + \frac{k}{t^2}\nabla^2 t + \text{ Radiation } . \tag{53}$$

Here, k is the coefficient of heat conduction, τ is time and, with Γ the effective viscosity, the viscous dissipation function Φ is given in tensorial form by [5]:

$$\Phi = \Gamma\left[\left(\frac{\partial u_i}{\partial x_j} + \frac{\partial u_j}{\partial x_i}\right)\frac{\partial u_i}{\partial x_j} - \frac{2}{3}\chi^2\right] , \tag{54}$$

where

$$\chi = \mathbf{div}\,\mathbf{u} . \tag{55}$$

Hence

$$Ds = \frac{\Phi}{\rho t}D\tau + \text{ conduction + radiation.} \tag{56}$$

Now, Ds is the entropy increase due to the mechanical work of the viscous forces, called Φ. For the present purposes what is needed is the *change* in the entropy increase due to small corrections to U and V which produce small corrections in Φ (neglect the effect of density corrections). In this case the conduction and radiation terms will be substantially unchanged and the entropy correction may be approximated by:

$$(Ds)' = \frac{\Phi'}{\rho t}D\tau . \tag{57}$$

Hence, substituting $(Ds)'$ into VH' and manipulating:

$$VH' = (\gamma - 1)D\tau\,\Phi' . \tag{58}$$

For $D\tau$, adopt the time a parcel of fluid remains in the reference volume, i.e., the transit time.

The changes in Φ due to U', V' are complex and tedious to compute. They are obtained starting from:

$$\Phi' = \frac{\partial\Phi}{\partial U_p}U_p' + \frac{\partial\Phi}{\partial U_w}U_w' + \frac{\partial\Phi}{\partial V_p}V_p' + \frac{\partial\Phi}{\partial V_s}V_s' . \tag{59}$$

To continue it is necessary to relate the face velocities to the velocity components in the appropriate coordinate system. For instance, for axisymmetric flow with swirl in cylindrical polar coordinates the expression for the time-averaged dissipation function reduces to [6][7]:

$$\Phi = \Gamma[2(U_x^2 + V_y^2 + (V/y)^2) + (U_y + V_x)^2 + w_x^2 + (w_x - w/y)^2 - \frac{2}{3}\chi^2] - \frac{2}{3}\rho\chi\kappa \ , \qquad (60)$$

where κ is the specific kinetic energy of the turbulence, w is the swirl component of velocity and

$$\chi = \mathbf{div}\,\mathbf{u} = U_x + V_y + V/y \ . \qquad (61)$$

There still remains to consider possible generalised coordinates. This has all been implemented but will not be detailed further. Assume the derivatives of Φ required in Eq (59) are known and define coefficients

$$ZU = \frac{VA}{c^2}(\gamma - 1)\Delta\tau\,\partial\Phi/\partial U \ , \qquad (62)$$

$$ZV = \frac{VA}{c^2}(\gamma - 1)\Delta\tau\,\partial\Phi/\partial V \ . \qquad (63)$$

Hence the remaining viscous heating terms may be put in the following form:

$$\begin{aligned} -\sum_{P,N,S,E,W}(\frac{VA}{c^2}VH') \ = \ & -ZV_pV_p' - ZV_sV_s' - ZU_pU_p' - ZU_wU_w' \\ & -ZV_nV_n' - ZV_pV_p' - ZU_nU_n' - ZU_{nw}U_{nw}' \\ & -ZV_sV_s' - ZV_{ss}V_{ss}' - ZU_sU_s' - ZU_{sw}U_{sw}' \\ & -ZV_eV_e' - ZV_{se}V_{se}' - ZU_eU_e' - ZU_pU_p' \\ & -ZV_wV_w' - ZV_{sw}V_{sw}' - ZU_wU_w' - ZU_{ww}U_{ww}' \ . \end{aligned} \qquad (64)$$

This may be efficiently organised by means of a subroutine which computes ZU and ZV at a generic cell location, and using the subroutine at cells N, S, E and W separately. Then, the computation at, for instance, N, would in fact be the computation of the second line of the above list; the correspondence is:

$$\text{Original:} \quad -ZV_nV_n' - ZV_pV_p' - ZU_nU_n' - ZU_{nw}U_{nw}' \ , \qquad (65)$$

$$\text{Computed at N:} \quad -ZV_pV_p' - ZV_sV_s' - ZU_pU_p' - ZU_wU_w' \ . \qquad (66)$$

That is, of the values computed at N keep $-ZV_s$ (to be added to the coefficient of V_p') and move all three others to the right-hand side.

The stencil of Fig 9 may assist in understanding this example. Note that it is not necessary to apply the subroutine at the centre cell.

The twelve terms $ZU\,U', ZV\,V'$ added to the RHS complete the desired function F. The viscous heating components to be added to coefficients a_1 to a_4 are:

$$-2ZV_s \text{ computed at N, add to } a_4 \text{ (i.e., for } V_p'), \tag{67}$$

$$-2ZU_w \text{ computed at E, add to } a_2 \text{ (i.e., for } U_p'), \tag{68}$$

$$-2ZV_p \text{ computed at S, add to } a_3 \text{ (i.e., for } V_s'), \tag{69}$$

$$-2ZU_s \text{ computed at W, add to } a_1 \text{ (i.e., for } U_w'). \tag{70}$$

Care must be taken in regions close to boundaries, where U, V and p are prescribed or otherwise fixed and there must be no computation of corrections.

Recapitulating, a routine is set up to compute the viscous heating terms (ZU, ZV). This routine is applied at the four adjacent cells (N, S, E, W) and components found for coefficients a_1 to a_4 and the right-hand side term F.

Coefficients a_1 to a_4 are completed by adding the appropriate density times area components $(\pm\rho^* DU, \pm\rho^* DV)$ as per Eqns. (24) to (27).

Coefficient a_5 is obtained as

$$\frac{VA}{c^2}\,|_P \ , \tag{71}$$

and all surrounding terms

$$\frac{VA}{c^2} p'\,|_{E,N,S,W} \tag{72}$$

are moved to the RHS.

Finally, the mass flow residual computed with current values of U, V and ρ is added to F.

The finished discretised continuity equation is:

$$a_1 U_w' + a_2 U_p' + a_3 V_s' + a_4 V_p' + a_5 p_P' = F \tag{73}$$

This form is suitable for all Mach numbers (within the limits of applicability of the transport equations), and for non-isentropic flows.

3.3 Discretising the Transport Equations

This Section considers improvements needed to the discretised transport equations; a brief description of the equations is given below.

The steady-state transport equation of a variable ϕ in generalised coordinates ξ, η, and integrated over the cell volume $d\mathcal{V}$ takes the form:

$$\frac{1}{J}\left[\frac{\partial(\rho U\phi)}{\partial\xi}+\frac{\partial(\rho V\phi)}{\partial\eta}\right]d\mathcal{V}=\frac{1}{J}\left[\frac{\partial}{\partial\xi}(C_1\frac{\partial\phi}{\partial\xi}+C_2\frac{\partial\phi}{\partial\eta})+\frac{\partial}{\partial\eta}(C_3\frac{\partial\phi}{\partial\eta}+C_4\frac{\partial\phi}{\partial\xi})\right]d\mathcal{V}+S^\phi d\mathcal{V}\,. \tag{74}$$

In these equations, U and V are the co-variant transformed velocities along the transformed axes ξ and η, J is the Jacobian of the transformation, Γ the coefficient of diffusion, S^ϕ the source term (generation/destruction of ϕ per unit volume per unit time) and other definitions are:

$$U = u\frac{\partial y}{\partial\eta}-v\frac{\partial x}{\partial\eta}\,, \tag{75}$$

$$V = v\frac{\partial x}{\partial\xi}-u\frac{\partial y}{\partial\xi}\,, \tag{76}$$

$$J = \frac{\partial x}{\partial\xi}\frac{\partial y}{\partial\eta}-\frac{\partial x}{\partial\eta}\frac{\partial y}{\partial\xi}\,, \tag{77}$$

$$d\mathcal{V} = JR\Delta\eta\Delta\xi\,, \tag{78}$$

$$C_1 = \Gamma\frac{(\partial x/\partial\eta)^2+(\partial y/\partial\eta)^2}{J}\,, \tag{79}$$

$$C_3 = \Gamma\frac{(\partial x/\partial\xi)^2+(\partial y/\partial\xi)^2}{J}\,, \tag{80}$$

$$C_2 = -\Gamma\frac{(\partial x/\partial\xi)(\partial x/\partial\eta)+(\partial y/\partial\xi)(\partial y/\partial\eta)}{J}\,, \tag{81}$$

$$C_4 = C_2\,. \tag{82}$$

Variable R is unity in a 2D Cartesian system, and equals the radial coordinate y in cylindrical polar coordinates.

The source term is usually assumed to be a linear function of the variable:

$$S^\phi = SU^\phi+\phi SP^\phi\,. \tag{83}$$

For the transport of variables u and v (i.e., velocities in the original system of coordinates x, y), the equations become the momentum transport or Navier-Stokes equations and the ensemble-averaged source terms, expressed in x, y coordinates for brevity, are (see, for instance, [6][7]):

$$S^u = -\frac{\partial p}{\partial x} + \frac{\partial}{\partial x}\left(\Gamma\frac{\partial u}{\partial x}\right) + \frac{\partial}{\partial y}\left(\Gamma\frac{\partial v}{\partial x}\right) - \frac{2}{3}\frac{\partial}{\partial x}(\Gamma\chi + \rho\kappa) + \frac{\Gamma}{y}\left(\frac{\partial u}{\partial y} + \frac{\partial v}{\partial x}\right) , \quad (84)$$

$$S^v = -\frac{\partial p}{\partial y} + \frac{\partial}{\partial x}\left(\Gamma\frac{\partial u}{\partial y}\right) + \frac{\partial}{\partial y}\left(\Gamma\frac{\partial v}{\partial y}\right) - \frac{2}{3}\frac{\partial}{\partial y}(\Gamma\chi + \rho\kappa) + \frac{2\Gamma}{y}\left(\frac{\partial v}{\partial y} - \frac{v}{y}\right) - \frac{2}{3}\frac{\rho\kappa}{y} + \frac{\rho w^2}{y} . \quad (85)$$

These equations are discretised using finite differences techniques and applied at the four faces of a cell. This procedure results in four Finite Differences Equations (FDE's) in five unknowns: the four face velocities and the pressure at the centre of the cell. When the continuity equation is added, the resulting 5x5 system can be solved for each cell.

Two problems need attention with regard to recirculating gas flows: securing compliance with the preset inlet boundary conditions and selecting a discretisation algorithm which maximises accuracy and secures convergence.

3.3.1 The Momentum equations near inlets

A brief description of the discretised transport equations and the method of solution is given below.

The discretised form of the 2D Navier-Stokes equations applied to the four faces of a cell is (from Refs [1] & [2]):

$$APU_w u_w + DU_w p_P = \sum_{N,S,E,W} (AiU_w u_i) + DU_w p_W + \partial p/\partial\eta \mid_w DU_w + SUU_w + SPU_w u_w , \quad (86)$$

$$APU_p u_p - DU_p p_P = \sum_{N,S,E,W} (AiU_p u_i) - DU_p p_E + \partial p/\partial\eta \mid_p DU_p + SUU_p + SPU_p u_p , \quad (87)$$

$$APV_s v_s + DV_s p_P = \sum_{N,S,E,W} (AiV_s v_i) + DV_s p_S + \partial p/\partial\xi \mid_s DV_s + SUV_s + SPV_s v_s , \quad (88)$$

$$APV_p v_p - DV_p p_P = \sum_{N,S,E,W} (AiV_p v_i) - DV_p p_N + \partial p/\partial\xi \mid_p DV_p + SUV_p + SPV_p v_p . \quad (89)$$

(In the References the pressure cross-derivatives $\partial p/\partial\eta$ and $\partial p/\partial\xi$ are included in the source term)

As in Section 3.2, DU and DV are the cell face areas, and p the static pressure. Lower case indices indicate cell faces and upper case indices indicate cell centres, except for the summations which are expanded as, for instance:

$$\sum_{N,S,E,W} (AiU_p u_i) = ANU_p u_n + AEU_p u_e + ASU_p u_s + AWU_p u_w . \quad (90)$$

In these equations APU, APV are the coefficients multiplying u and v as a result of the discretisation process; the subindex indicates the face at which they are computed. Surrounding velocities u_i and v_i are grouped on the RHS, multiplied by similar coefficients AiU and AiV, where i stands for the four surrounding cells N, S, E and W.

Generalised coordinates (ξ,η) are used, which explains the pressure cross-derivatives; for instance the first equation, which is the U or ξ momentum equation, contains a derivative with respect to η. Because boundary-fitted coordinates are often fairly well aligned with the flow, these derivatives are usually numerically small and are not manipulated further; they are later added to the residuals.

The source terms are given in a linear form for the sake of completeness, comprising an independant source term (SUU, SUV) computed at the ceil face, and a term linearly proportional to velocity (SPU, SPV). For the Navier-Stokes equations SPU and SPV are zero.

The current values of the primitive variables u^*, v^* and p^* do not satisfy the system of FDE's, and a residual can be computed equal to the left-hand side minus the right-hand side of each equation computed with current values. Then, substituting the correction expressions:

$$u = u^* + u' , \tag{91}$$
$$v = v^* + v' , \tag{92}$$
$$p = p^* + p' , \tag{93}$$

there result the correction equations:

$$APU_w u'_w + DU_w p'_P = \sum_{N,S,E,W} (AiU_w u'_i) + DU_w p'_W + RU_w , \tag{94}$$
$$APU_p u'_p - DU_p p'_P = \sum_{N,S,E,W} (AiU_p u'_i) - DU_p p'_E + RU_p , \tag{95}$$
$$APV_s v'_s + DV_s p'_P = \sum_{N,S,E,W} (AiV_s v'_i) + DV_s p'_S + RV_s , \tag{96}$$
$$APV_p v'_p + DV_p p'_P = \sum_{N,S,E,W} (AiV_p v'_i) - DV_p p'_N + RV_p , \tag{97}$$

where RU, RV are the residuals.

As mentioned above, a 5x5 system of ordinary FDE's is obtained (called the Block Implicit System) which can be arranged as:

$$\begin{bmatrix} a_{11} & 0 & 0 & 0 & a_{15} \\ 0 & a_{22} & 0 & 0 & a_{25} \\ 0 & 0 & a_{33} & 0 & a_{35} \\ 0 & 0 & 0 & a_{44} & a_{45} \\ a_{51} & a_{52} & a_{53} & a_{54} & a_{55} \end{bmatrix} \begin{bmatrix} u'_w \\ u'_p \\ v'_s \\ v'_p \\ p_P \end{bmatrix} = \begin{bmatrix} F_1 \\ F_2 \\ F_3 \\ F_4 \\ F_5 \end{bmatrix} \begin{array}{l} u\text{-momentum at } w , \\ u\text{-momentum at } p , \\ v\text{-momentum at } s , \\ v\text{-momentum at } p , \\ \text{Continuity} . \end{array} \tag{98}$$

Coefficients a_{ij} can be identified by comparison with the FDE's; for instance, for the u-momentum equation at the w face:

$$a_{11} = APU_w \,, \tag{99}$$
$$a_{15} = DU_w \,, \tag{100}$$

and for the continuity equation (Eq. (73), Section 3.2.2), the correspondence is $a_{51} = a_1$, $a_{52} = a_2$, etc.

This system is solved for each cell. Then, all cells are solved in one sweep of the flow region (note that the solutions are transported between cells since, e.g., u'_p of one cell becomes u'_w of the adjacent cell to the right, and various u', v' and p' are placed on the RHS's of other cells). The whole field is then swept repeatedly until a converged solution is found, indicated by a reduction of the residuals to acceptable levels.

New values of the primitive variables are then found as:

$$u = u^* + u' \,, \tag{101}$$
$$v = v^* + v' \,, \tag{102}$$
$$p = p^* + p' \,, \tag{103}$$
$$\rho = \rho^* + \frac{(p' - VH')}{c^2} \,. \tag{104}$$

This completes the brief presentation of the discretised transport equations and the method of solution.

A particular problem arises near boundaries, where primitive variables are specified and are not to be corrected. For instance, if the w face is a solid wall the following must be complied with:

$$u^*_w = u'_w = 0 \,, \tag{105}$$
$$v^*_w = v'_w = 0 \,. \tag{106}$$

This is catered for by making, in this case, $a_{11} = 1$, $a_{15} = F_1 = 0$. This yields $u'_w = 0$, and the value of u_w will be unperturbed (i.e., will continue to be zero as set initially). However, p'_P is now disconnected from the u-momentum at the w face, i.e., from the prescribed boundary values.

This introduces the problem of prescribed boundary values. The necessary and sufficient conditions at boundaries for compressible viscous flows are not theoretically known, and boundary conditions are usually specified in an *ad hoc* manner. Since the conservation of

momentum and energy equations are to be satisfied the values of u, v, and t are set, either by Neumann (gradient) or Dirichlet (value) conditions.

As the continuity equation must also be satisfied and u and v have been set, the last value to be specified is density or, since continuity has been put in pressure-velocity terms, pressure.

For solid wall-, outlet- and symmetry-type boundaries the last condition is a simple Neumann condition:

$$\frac{\partial p}{\partial n} = 0 \ (n = \text{normal to boundary}) \ . \tag{107}$$

This is effected by making the pressure at the boundary equal to the pressure at the first inner cell centre.

This, however, leaves the general pressure level totally free. Inlet-type boundaries are the only means left to link the pressure levels over the whole field to the fluid inlet conditions. Hence, a Neumann condition is applied in reverse, i.e., the boundary pressure is given and the first inner cell centre forced to this value. In the correction system p' would be forced to

$$p' = p_{boundary} - p^* \ . \tag{108}$$

This is the usual procedure, i.e., to assume no streamwise static pressure gradient at the inlet, and becomes more satisfactory as the mesh is made finer. In the multigrid system, however, quite coarse meshes may be used, and the assumption is not satisfactory.

To achieve a better inlet boundary condition specification, start again from the second law:

$$\frac{ds}{C_p} = \frac{dt}{t} - \frac{\gamma - 1}{\gamma}\frac{dp}{p} \ . \tag{109}$$

Since the transformation between static and stagnation states is by definition isentropic this may also be written:

$$\frac{ds}{C_p} = \frac{dT}{T} - \frac{\gamma - 1}{\gamma}\frac{dP}{P} \ . \tag{110}$$

It is assumed that at the inlet the flow will not be reacting, and that the enthalpy difference between cells is relatively small, whence heat transfer by radiation and conduction *between cells at the inlet* is negligible. Then:

$$\frac{dT}{T} = 0 \ . \tag{111}$$

Also, as before,

$$ds = \frac{\phi}{\rho t} d\tau \ . \tag{112}$$

Substituting and manipulating:

$$\frac{dP}{d\tau} = -\frac{P}{p}\phi \ . \tag{113}$$

In generalized coordinates:

$$\frac{dP}{d\tau} = u\frac{\partial P}{\partial x} + v\frac{\partial P}{\partial y} \ , \tag{114}$$

$$\frac{\partial P}{\partial x} = \frac{1}{J}\left(\frac{\partial y}{\partial \eta}\frac{\partial P}{\partial \xi} - \frac{\partial y}{\partial \xi}\frac{\partial P}{\partial \eta}\right) \ , \tag{115}$$

$$\frac{\partial P}{\partial y} = \frac{1}{J}\left(\frac{\partial x}{\partial \xi}\frac{\partial P}{\partial \eta} - \frac{\partial x}{\partial \eta}\frac{\partial P}{\partial \xi}\right) \ , \tag{116}$$

$$u = \frac{1}{J}\left(\frac{\partial x}{\partial \xi}U + \frac{\partial x}{\partial \eta}V\right) \ , \tag{117}$$

$$v = \frac{1}{J}\left(\frac{\partial y}{\partial \xi}U + \frac{\partial y}{\partial \eta}V\right) \ . \tag{118}$$

Substituting and manipulating:

$$\frac{1}{J}\left(U\frac{\partial P}{\partial \xi} + V\frac{\partial P}{\partial \eta}\right) = -\frac{P}{p}\phi \ . \tag{119}$$

If ξ and η are boundary-fitted coordinates and the inlet boundary has been sensibly chosen (i.e., with minimal divergence of the velocity vector), one of the coordinates (say, ξ) will be substantially aligned with the flow. Focusing then on $\partial P/\partial \xi$ (Fig 10):

$$\frac{\partial P}{\partial \xi} = \frac{P - P_W}{\Delta \xi / 2} \ . \tag{120}$$

Substituting and rearranging:

$$P\left(1 + \frac{\phi J}{p}\frac{\Delta \xi}{2U}\right) = P_W - \frac{V}{U}\frac{\partial P}{\partial \eta}\frac{\Delta \xi}{2} \ . \tag{121}$$

Since time is invariant:

$$J\Delta \xi / U \simeq \Delta x / u \simeq \Delta \tau \ . \tag{122}$$

This yields:

$$P = \frac{P_W - \frac{V}{U}\frac{\partial P}{\partial \eta}\frac{\Delta \xi}{2}}{1 + \frac{\phi \Delta \tau}{2p}} \,. \tag{123}$$

This equation links the total pressure at the first cell centre P to the total pressure at the inlet P_W. There is a total pressure drop due to the work of the viscous forces (the denominator is always larger than unity). The second term in the numerator represents transport from adjacent cells into the control volume of fluid with a different total pressure, in the transverse direction. In the conventionally positive case, for example, with flow from bottom to top, $V/U > 0$, $\partial P/\partial \eta < 0$, and there is a net contribution which reduces the total pressure loss.

The expression allows calculation of P and hence the static pressure, from where the pressure correction is calculated as:

$$p' = p_{calculated} - p^* \,. \tag{124}$$

This is an exact formulation and is hence applicable to the coarsest meshes. In practice it is found sufficient to enforce it on the finest meshes and leave the coarsest meshes free, which appears to accelerate convergence.

3.3.2 The Power-Law scheme

This Section describes improvements made to the procedure used to generate the coefficients *in the discretised transport equations.*

The coefficients of u and v in the transport FDE's are AiU, AiV and APU, APV, where i stands for the four surrounding centres E, W, N and S, and the last two coefficients are obtained by summing:

$$APU = \sum_{N,E,S,W} (AiU) \,, \tag{125}$$

$$APV = \sum_{N,E,S,W} (AiV) \,. \tag{126}$$

Expressions for these coefficients vary according to the differencing scheme adopted to convert the Partial Differential Equations (e.g., the Navier-Stokes equations) into Finite Differences Equations. If, for instance, a Taylor series expansion centred on the cell face is used, the result is known as the **Central Differences** scheme, and the coefficients are, for example

$$AEU = DX - CX \,, \tag{127}$$

$$AWU = DX + CX \,, \tag{128}$$

$$ANU = DY - CY \,, \tag{129}$$

$$ASU = DY + CY \,, \tag{130}$$

where, disregarding coordinate transformation metrics, the Convection coefficients CX, CY and the Diffusion coefficients DX, DY are:

$$CX = \frac{1}{2}\rho U\, DU\,, \tag{131}$$

$$CY = \frac{1}{2}\rho V\, DV\,, \tag{132}$$

$$DX = \frac{\Gamma DU}{\Delta y}\,, \tag{133}$$

$$DY = \frac{\Gamma DV}{\Delta x}\,. \tag{134}$$

A detailed discussion of this scheme may be found in [8], where it is also shown that when the cell Peclet number

$$Pe = \frac{2CX}{DX} \tag{135}$$

exceeds 2 in absolute value the solution may become unstable.

There are a several methods which may be used to restrict the excursions in the Central Difference scheme whilst maintaining the desirable characteristics of the scheme, i.e., ability to compute reversing flows, and second-order accuracy. Incorporation of such methods to MULTIFLOW-2D is not currently envisaged since the multigrid system allows the use of very fine grids, and gas turbine combustion does not involve relatively high gas velocities.

Stability may be secured by resorting to the **Upwind Differencing** scheme, where the convection terms are discretized using the principle that the value of the variable at the cell face equals the value at the upwind cell centre, much as was described in Section 3.2.1 for density. Diffusion terms are discretized as above. This scheme is less accurate, and unsuitable for recirculating flows, but may be acceptable since it will be used in the coarse grids, and in regions of flow where convection is dominant.

In this case the coefficients become, for example:

$$AEU = DX + M[-2CX]\,, \tag{136}$$

$$AWU = DX + M[+2CX]\,, \tag{137}$$

where M is the MAX operator defined before (Section 3.2.1). For example, if $CX > 0$ (conventionally positive U), two coefficients CX are added to the upwind side (AWU) and none to the downwind side (AEU), compared to one each in the Central Differences scheme.

The original version of MULTIFLOW-2D incorporated these considerations by means of computing the coefficients in one or the other manner according to the value of the Peclet number. This is known as the **Hybrid Scheme** of discretisation.

This was found unsatisfactory in the multigrid environment: since each grid is twice the size of the next finer grid, it is possible for regions of flow to exist where the cell Peclet number oscillates around 2, and different discretization schemes are used in contiguous grids. In these cases information transfers between grids not only do not help convergence, but may lead to divergence.

Patankar [8] has shown that an exact solution (at least in one-dimensional transport) involves not an on/off change between schemes but a smooth transition via an exponential function of the Peclet number; he has also given an empirical approximation to the exact solution. With this the coefficients can be written:

$$AEU = DX\,A(|\,Pe\,|) + M[-2CX]\,, \tag{138}$$

$$AWU = DX\,A(|\,Pe\,|) + M[+2CX]\,, \text{etc.}, \tag{139}$$

where the **Power-Law** function A is given by:

$$A(|\,Pe\,|) = M[\left(1 - \frac{|\,Pe\,|}{10}\right)^5]\,. \tag{140}$$

This has been incorporated into the code.

The Power-Law has also been applied to the generalised transport equations for scalars such as enthalpy and mixture fraction, and particularly to the $\kappa - \epsilon$ turbulence model. The modification requires the inclusion of Prandtl numbers σ so that the diffusion coefficients become DX/σ, DY/σ, and

$$Pe = \frac{2\sigma CX}{DX}\,, \text{etc.} \tag{141}$$

4. APPLICATION EXAMPLES

4.1 Jet in a sudden expansion

The first example is chosen to show the ability to compute strongly recirculating flows. A circular jet 0.12 m in diameter enters a circular duct 0.6 m in diameter and 2.4 m long. Inlet conditions are:

- Reference inlet velocity U_0= 200 m/sec,
- v= 0,

- p= 104429 Pa,
- T= 300 K.

A 1/7th-power velocity distribution law is assumed at the jet inlet, formulated to yield the same volumetric flow rate as U_0. Hence, inlet axial velocity at a radius r is given by:

$$U = \frac{120}{98}\left(1 - \frac{r}{R}\right)^{1/7} U_0 \text{ , with } R\text{= 0.06 .} \tag{142}$$

Inlet turbulence is set at 5% of U for all components:

$$\kappa = \frac{\overline{u'^2} + \overline{v'^2} + \overline{w'^2}}{2} \simeq \frac{3}{2}(0.05\,U)^2 \text{ .} \tag{143}$$

Hence static temperature:

$$t = T - \frac{U^2 + 2\kappa}{2\,C_p} \text{ , with } C_p\text{= 1000 m}^2\text{/sec}^2\text{K .} \tag{144}$$

Whence density:

$$\rho = p/Rt \text{ , with } R\text{= 286.7 m}^2\text{/sec}^2\text{K .} \tag{145}$$

Turbulence scale length is set at $L = R/2$. Hence, with C_D= 0.09 :

$$\epsilon = C_D^{3/4}\frac{\kappa^{3/2}}{L} \text{ .} \tag{146}$$

With the above, inlet conditions at the centreline are:

$$\begin{aligned} U &= 245\text{m/sec ,} \\ \kappa &= 225\text{m}^2\text{/sec}^2\text{ ,} \\ t &= 269.8\text{K ,} \\ \rho &= 1.3485\text{kg/m}^3\text{ ,} \\ \epsilon &= 18485\text{m}^2\text{/sec}^3\text{ ,} \\ M &= 0.75\text{ .} \end{aligned}$$

The finest computational mesh has 240x32 cells, and there are three lower grid levels, i.e., coarse grids of 30x4, 60x8 and 120x16 cells.

Computation results are shown in Figures 11 to 14. Fig 11 shows the upper half of the duct with flow trajectories obtained by integration of the velocity vectors. The centre jet enters at left with a 0.06 m radius.

Fig 12 is a close-up view of the region near the inlet, where a small counter-rotating vortex is visible at the corner, to give an indication of the fineness of detail obtainable.

Fig 13 shows contours of turbulent kinetic energy κ; note the closely packed contour lines between the centreline and R at $x \simeq 0.5$. Turbulence intensities can be computed from κ as:

$$u' \simeq \sqrt{\frac{2}{3}\kappa} \tag{147}$$

Expressed as a fraction of centreline velocities, turbulence intensities range from 13% near the inlet to 71% near the outlet.

Turbulent kinetic energy is also plotted as a 3D carpet plot in Fig 14, with the jet entering from right to left at the origin (0,0). This representation evidences the horseshoe pattern of the peak TKE, which is not obvious in Fig 13, and was only suggested by the packed contour lines.

The code performance is deemed satisfactory, in that it yields plausible flow structures with the expected features (such as recirculation zones and shear layers), and fine detail.

4.2 Axisymmetric Contraction

The second example is a design verification exercise of a contracting circular duct. Duct diameters are 0.525 m at the inlet and 0.135 m at the outlet; duct length is 0.62 m. The duct profile was designed by others, and it is desired to verify that this shape can accelerate a flow of air by approximately an order of magnitude without risking separation and with uniform discharge velocity.

Inlet conditions are iteratively adjusted to obtain $M \simeq 0.8$ at the outlet and a properly expanded flow (outlet static pressure approximately atmospheric). Inlet velocity is a nominal 13 m/sec, with a 1/7th-power radial distribution and 5% turbulence. Three mesh levels were used with 17x4, 34x8 and 68x16 cells.

Computation results are shown in Figures 15 to 19. Fig 15 shows true streamlines (surfaces enclosing a given mass flow, as distinct from the flow trajectories of Fig 11). Thickening of the 90%-100% layer in the concave region is modest, indicating a low probability of separation. There are no indications of reversed or separated flow.

Contours of axial velocity (Fig 16) are nearly circular in the approach region, which is taken as an indication of a satisfactory design in that fluid parcels at similar distances from the outlet possess the same velocity. The exit velocity distribution is quite uniform (Fig 17), and the exit Mach number is approximately 0.8.

Turbulence intensity is low throughout: from the inlet value of 5% it drops to approximately 2% at the outlet (Fig 18).

Fig 19 shows that the radial static pressure gradient at the outlet is low, indicating a substantially parallel outlet flow.

Detailed analysis of these numerical simulation results and comparisons with the physical experiment will be reported elsewhere. Nevertheless it may be said that the simulation shows the duct design to be satisfactory.

5. CONCLUSIONS

A computer program named MULTIFLOW-2D has been acquired for use at ARL. This program, which is capable of computing numerical simulations of internal reactive flows, has been thoroughly analysed and refined. Important improvements relevant to gas turbine combustion have been developed and incorporated, such as the ability to compute flows with variable density and also non-isentropic flows. Code development has reached the stage where it can be applied with confidence to practical problems.

Until now development has been focused on the aerothermodynamics aspects of the code. Development of the reactive flow facilities (chemistry, kinetics) should now proceed as is planned. As a matter of detail, it is intended to reassess the possible incorporation of limiting schemes during later development stages, to dispense with the Power-Law scheme. This may be appropriate, for instance, if a need arises to use higher order discretisation algorithms.

6. REFERENCES

1 VANKA, S. P.; "MULTIFLOW-2D - A computer Program for Analysis of Two-dimensional Planar and Axisymmetric Turbulent Reacting Flows"; Draft Report, Advanced Propulsion Laboratory, WPAFB, Ohio, undated.

2 VANKA, S. P.; "Analytical studies of Three-dimensional combustion processes"; Report No AFWAL-TR-88-2140, Aero Propulsion and Power Laboratories, WPAFB, Ohio, May 1989.

3 BRIZUELA, E. A.; "An appraisal of the options for the numerical simulation of reactive flows in confined regions"; Propulsion Note No 6/92, Flight Mechanics and Propulsion Division, ARL, September 1992.

4 KARKI, K. C., and PATANKAR, S. V.; "Pressure-based calculation procedure for viscous flows at all speeds in arbitrary configurations"; *AIAA Journal*, Vol 27, N0 9, Pages 1167-1174, September 1989.

5 HUGHES, W. F., and BRIGHTON, J. A.; "Fluid Dynamics", Schaum Pub. Co., New York, 1967.

6 PAI, S.; "Viscous Flow Theory"; Van Nostrand, New York, 1957.

7 JOHNSTON, L. J; "Solution of the Reynolds-averaged Navier-Stokes equations for transonic aerofoil flows"; *Aeronautical Journal*, Pages 253-273, October 1991.

8 PATANKAR, S. V.; "Numerical heat transfer and fluid flow"; Hemisphere Publishing Co., New York, 1980.

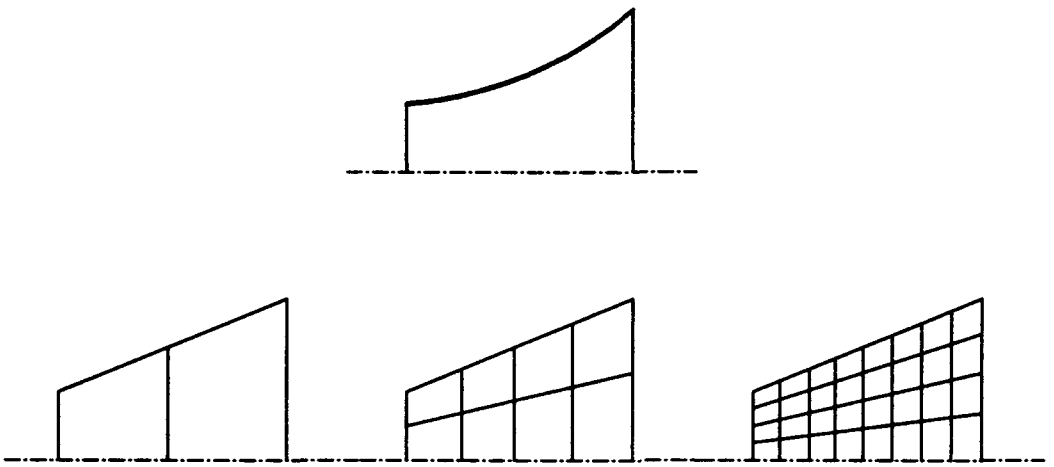

Axisymmetric expanding duct with 2x1 coarse grid
and next two fine grids (original scheme)

FIG 1

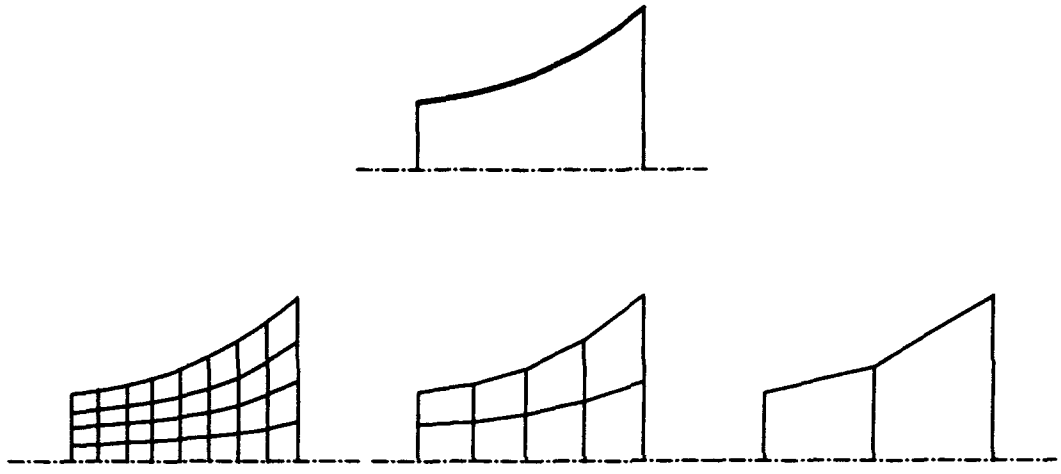

Axisymmetric expanding duct with 8x4 fine grid
and next two coarse grids (revised scheme)

FIG 2

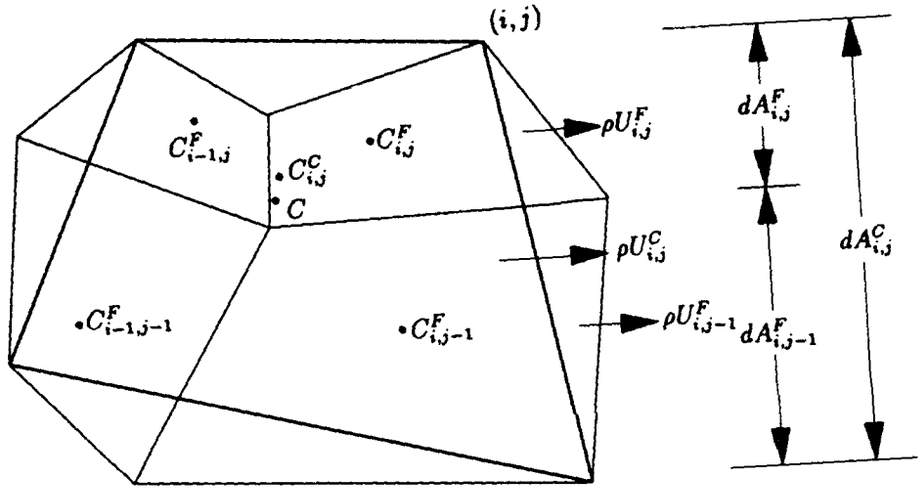

Transfers between fine and coarse meshes

FIG 3

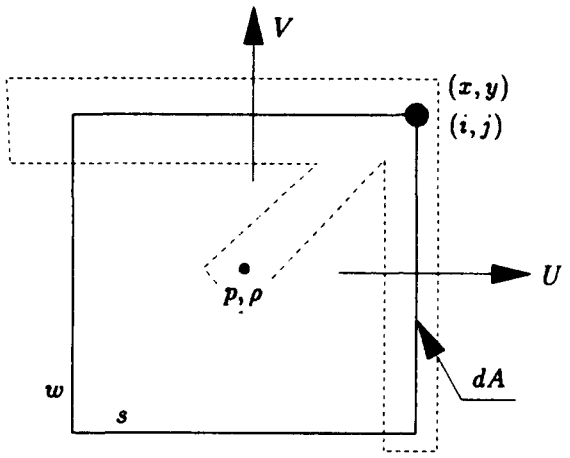

Staggered grid variable location

FIG 4

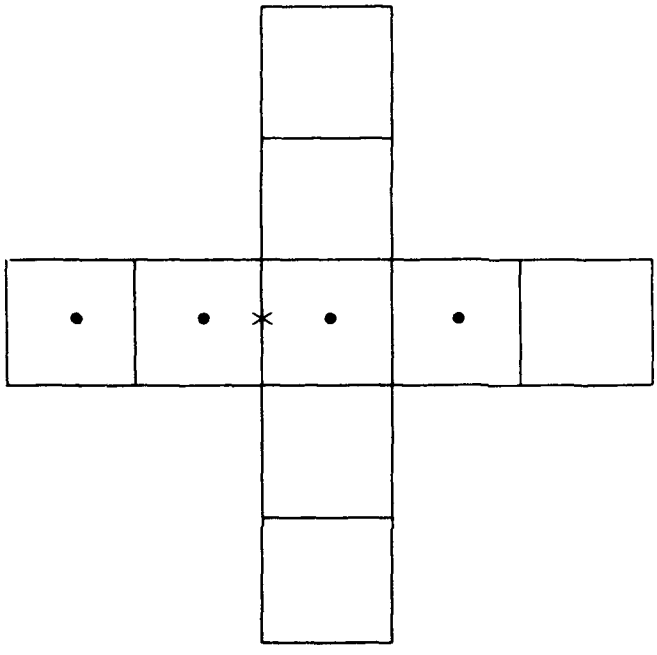

Stencil for spline fitting

FIG 5

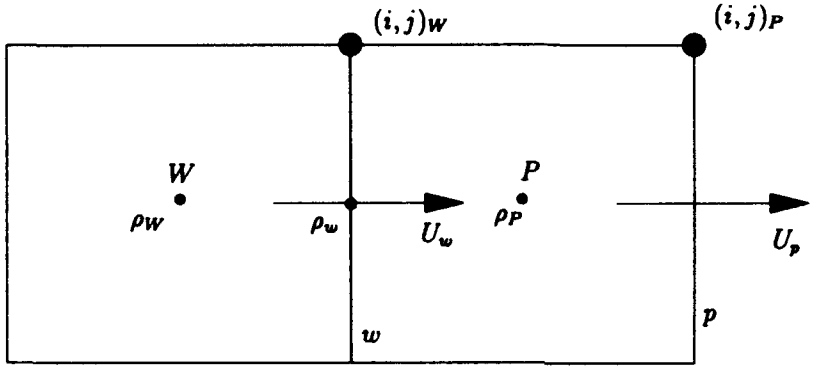

Karki and Patankar scheme

FIG 6

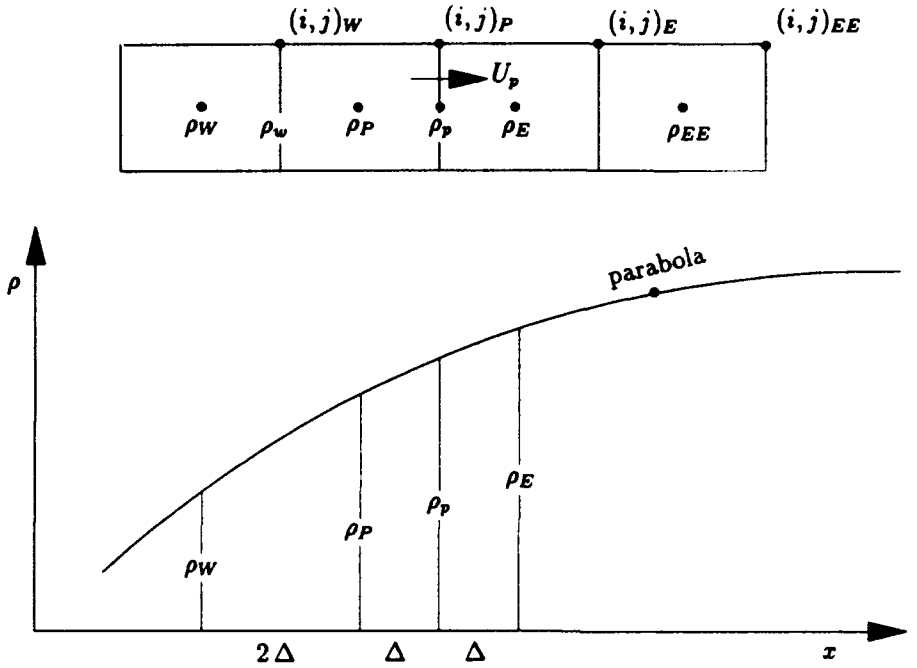

Upwind-biased second-order interpolation

FIG 7

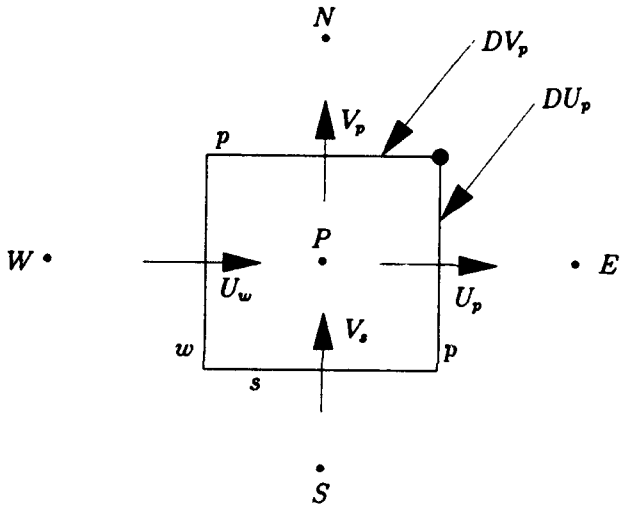

Computation locations

FIG 8

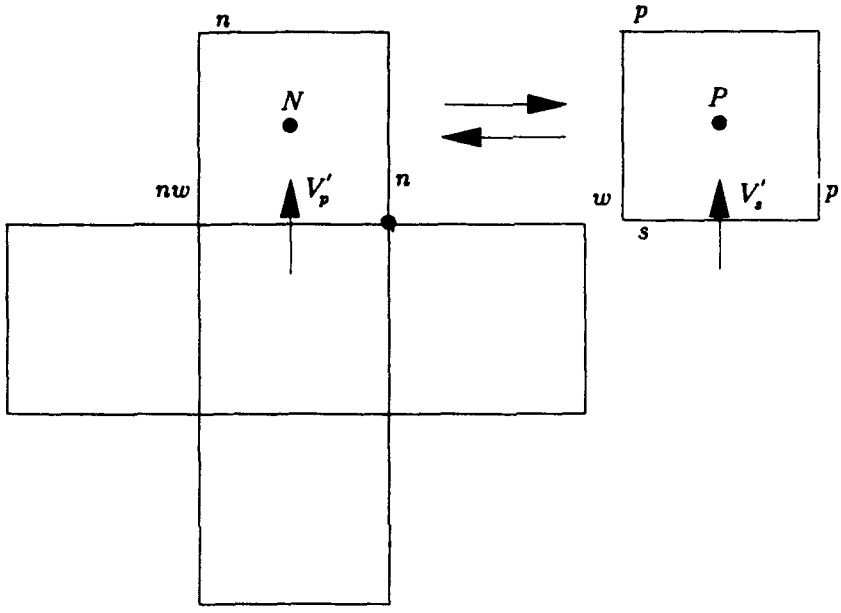

Stencil for Viscous Heating contributions

FIG 9

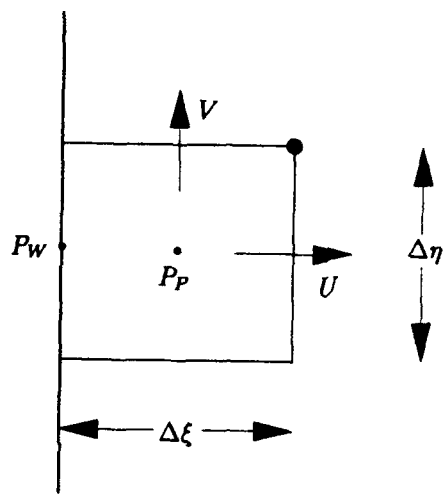

Inlet-type boundary at w-face and boundary-fitted coordinates

FIG 10

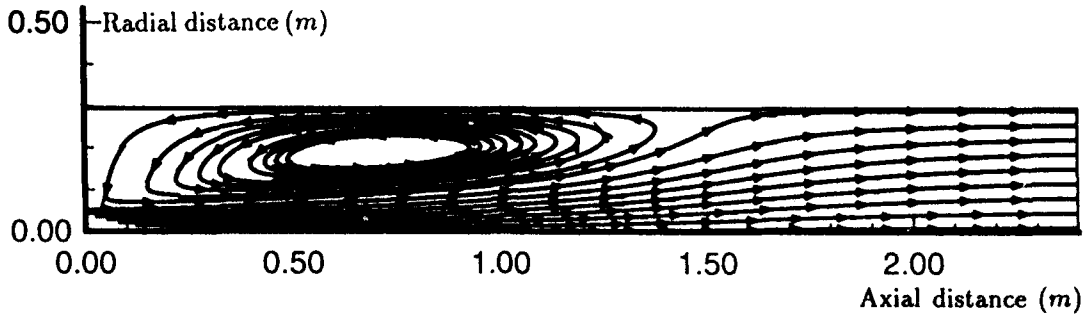

Jet in an expanding duct
Flow trajectories

FIG 11

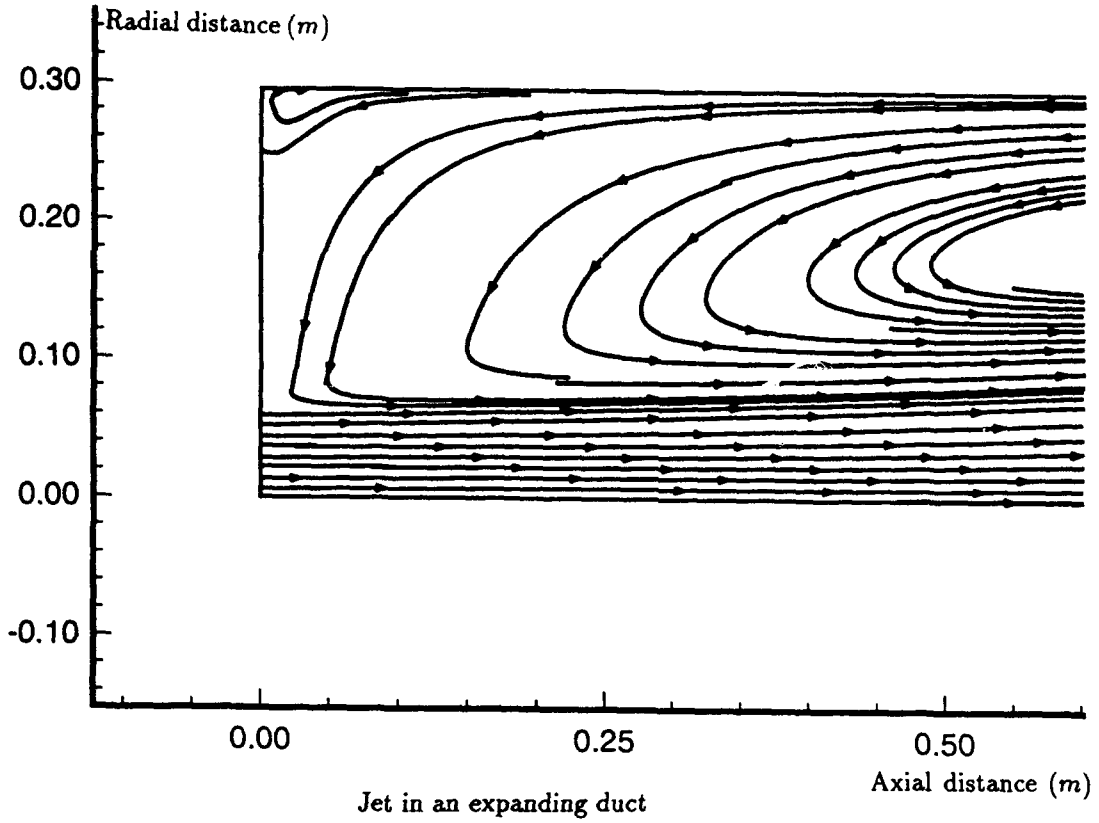

Jet in an expanding duct
Flow trajectories (close-up)

FIG 12

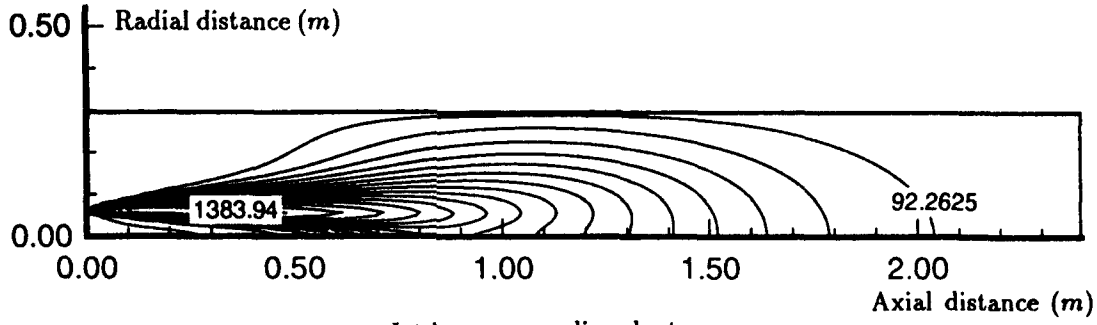

Jet in an expanding duct
Contours of Turbulent Kinetic Energy (m^2/sec^2)

FIG 13

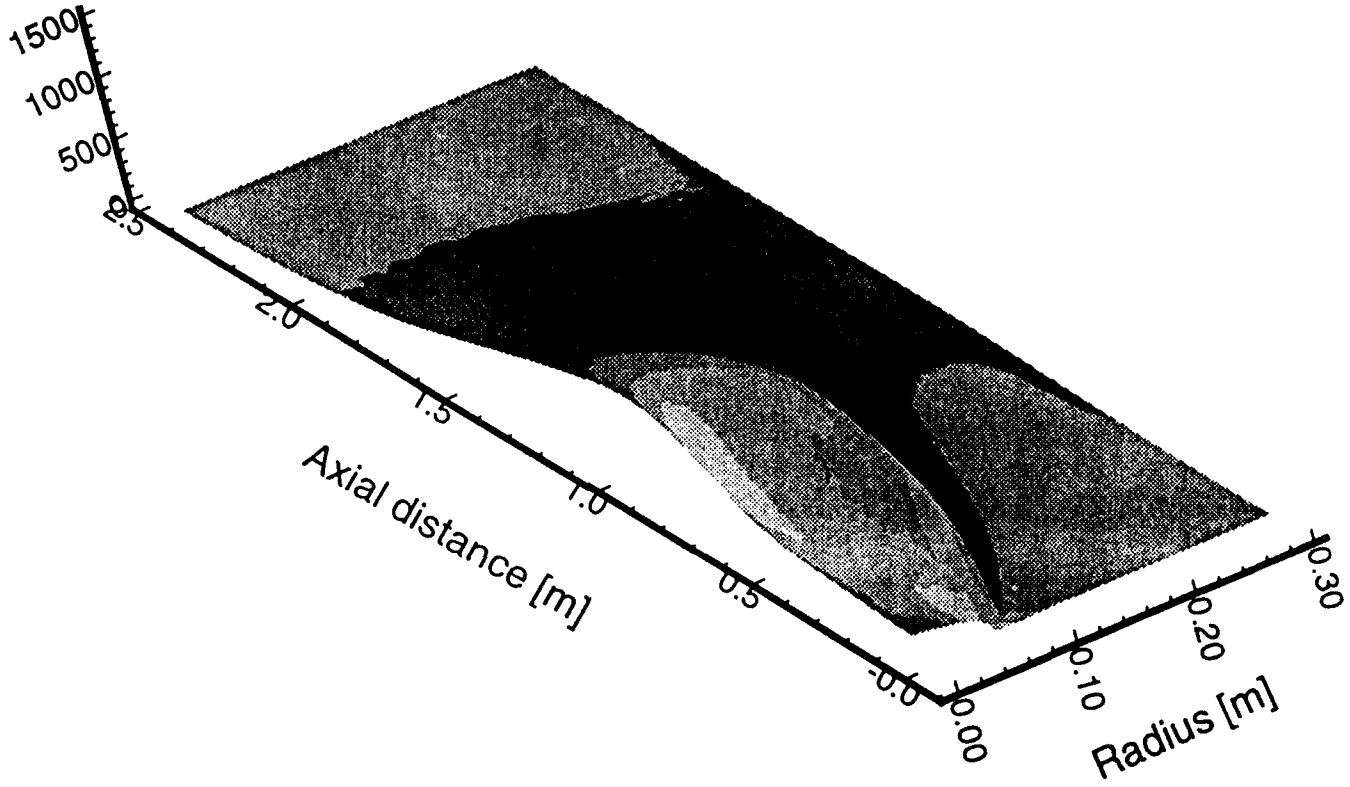

Jet in an expanding duct
3D plot of Turbulent Kinetic Energy (m^2/sec^2)
FIG 14

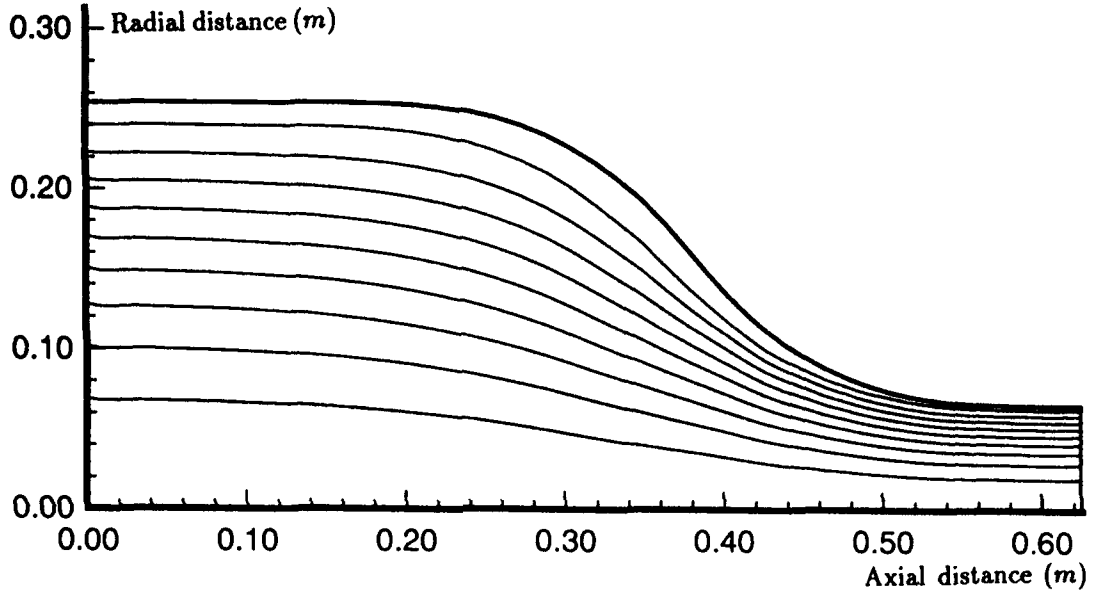

Axisymmetric contraction
Contours of mass flow (every 10%)

FIG 15

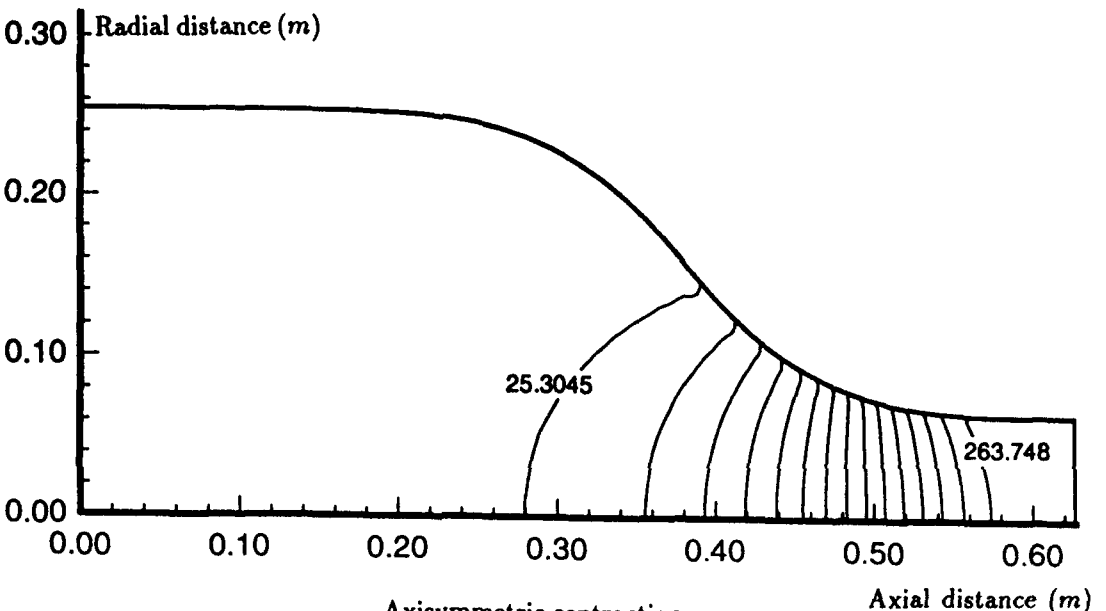

Axisymmetric contraction
Contours of constant axial velocity (m/sec)

FIG 16

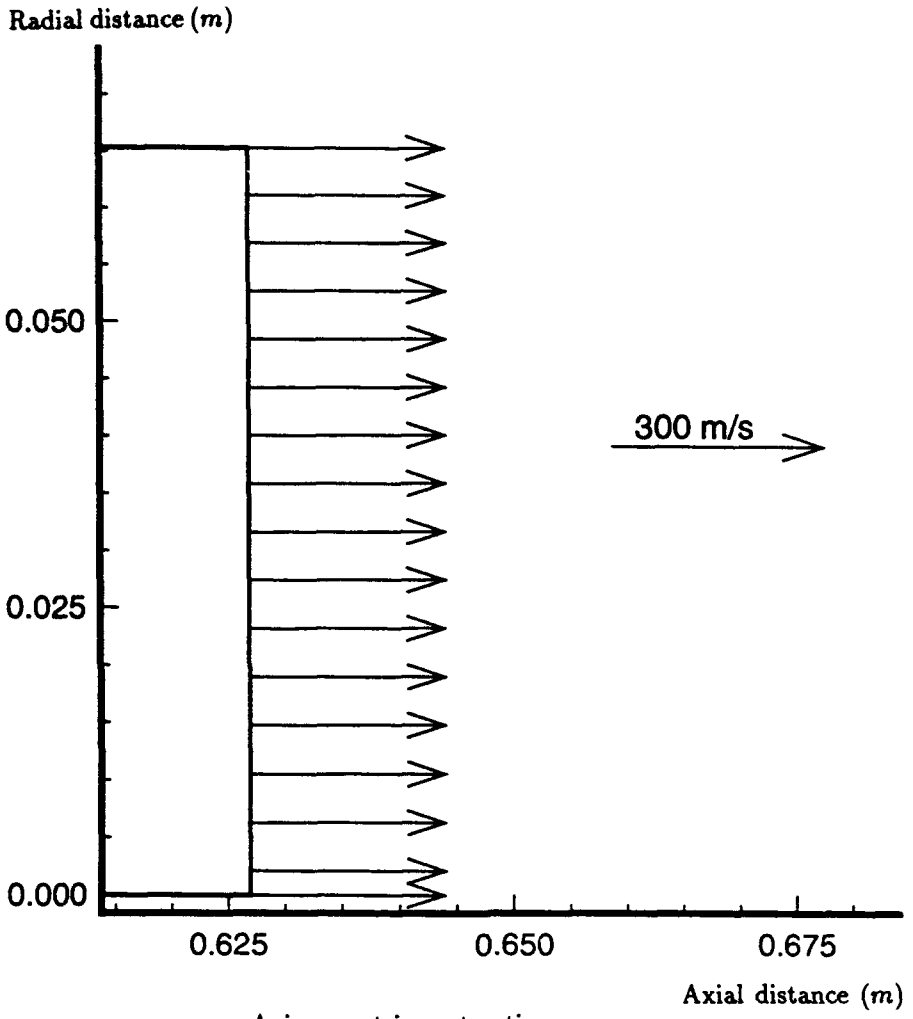

Axisymmetric contraction
Exit velocity vectors (scale indicated)

FIG 17

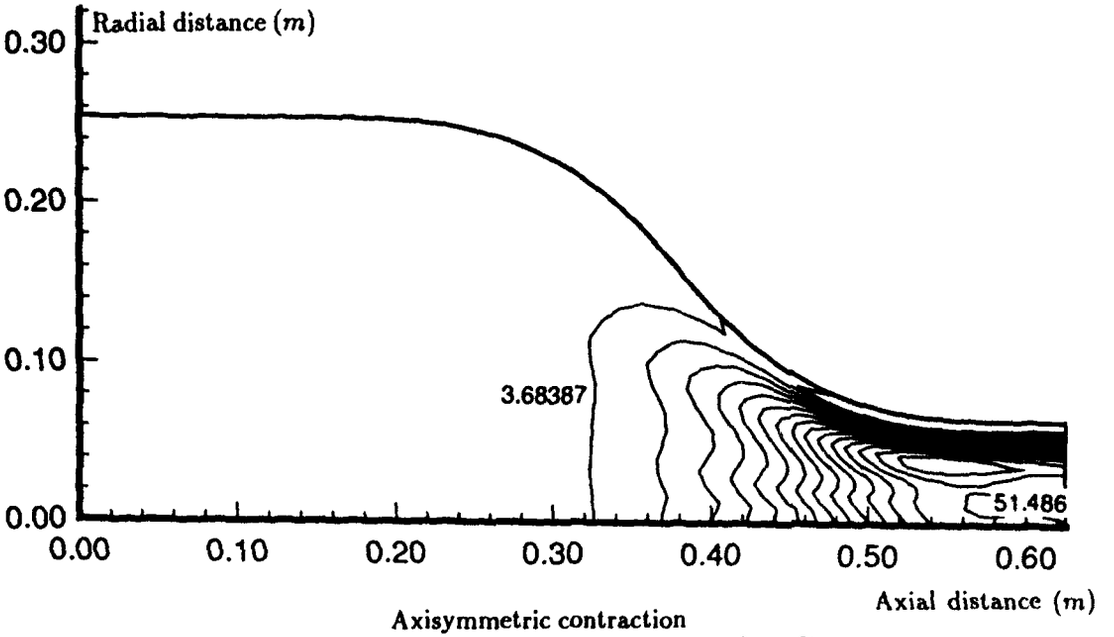

Axisymmetric contraction
Contours of Turbulent Kinetic Energy (m^2/sec^2)

FIG 18

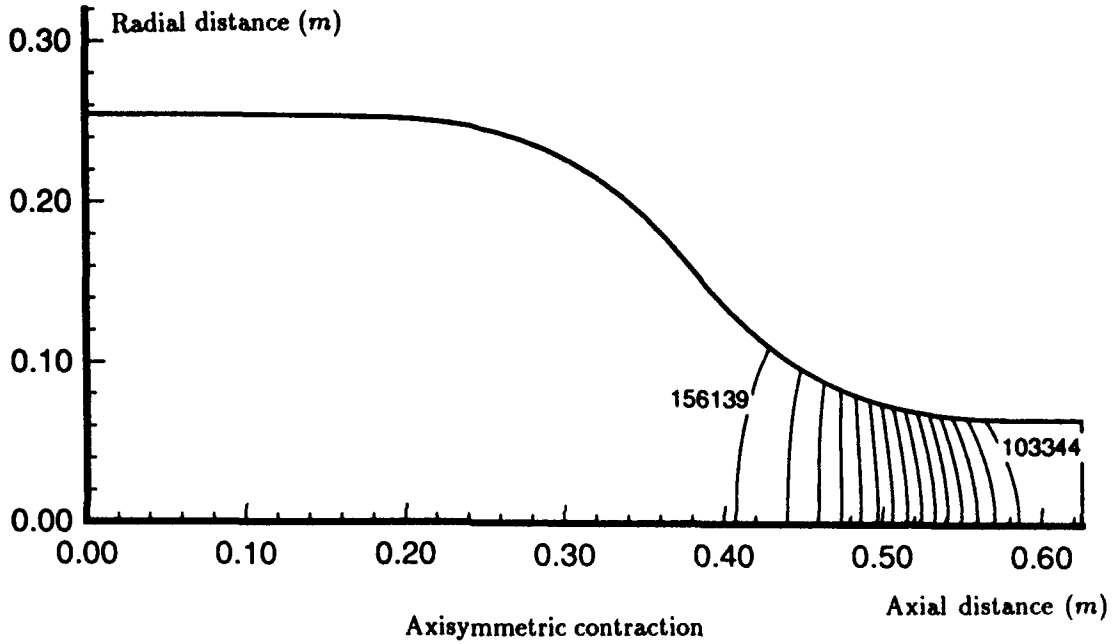

Axisymmetric contraction
Contours of static pressure (Pa)

FIG 19

DISTRIBUTION

AUSTRALIA

DEFENCE ORGANISATION

Defence Science and Technology Organisation

Chief Defence Scientist
FAS Science Policy
AS Science Corporate Management
} shared copy

Counsellor Defence Science, London (Doc Data Sheet only)
Counsellor Defence Science, Washington (Doc Data Sheet only)
Senior Defence Scientific Adviser (Doc Data Sheet only)
Scientific Advisor Policy and Command (Doc Data Sheet only)
Navy Scientific Adviser (3 copies Doc Data Sheet only)
Scientific Adviser - Army (Doc Data Sheet only)
Air Force Scientific Adviser (Doc Data Sheet only)
Scientific Adviser to Thailand MRD (Doc Data sheet only)
Scientific Adviser to the DRC (Kuala Lumpur) (Doc Data sheet only)

Aeronautical Research Laboratory
Director
Library
Chief Airframes and Engines Division
Author: E. Brizuela
Propulsion File

Materials Research Laboratory
Director/Library

Main Library - DSTO Salisbury

Defence Central

OIC TRS, Defence Central Library
Document Exchange Centre, DSTIC (8 copies)
Defence Intelligence Organisation
Library, Defence Signals Directorate (Doc Data Sheet Only)

HQ ADF
Director General Force Development (Air)

Navy
Director Aircraft Engineering - Navy

Army
Engineering Development Establishment Library
Director Aviation - Army

Air Force

Aircraft Research and Development Unit
Scientific Flight Group
Library
DTA-LC
DENGPP-AF
OIC ATF, ATS, RAAFSTT, WAGGA (2 copies)

UNIVERSITIES AND COLLEGES

Australian Defence Force Academy
Library
Head of Aerospace and Mechanical Engineering

Flinders
Library

LaTrobe
Library

Melbourne
Engineering Library

Monash
Hargrave Library

Newcastle
Library

New England
Library

Sydney
Engineering Library

NSW
Physical Sciences Library
Head, Mechanical Engineering

Queensland
Library

Tasmania
Engineering Library

Western Australia
Library
Head, Mechanical Engineering

RMIT
Library
Mr M.L. Scott, Aerospace Engineering

University College of the Northern Territory
Library

OTHER GOVERNMENT DEPARTMENTS AND AGENCIES

AGPS
Gas & Fuel Corporation of Vic., Manager Scientific Services
SEC of Vic., Herman Research Laboratory, Library
Australian Nuclear Science and Technology Organisation
CSIRO DBCF

OTHER ORGANISATIONS

NASA (Canberra)
ASTA Engineering, Document Control Office
Hawker de Havilland Aust Pty Ltd, Victoria, Library
Hawker de Havilland Aust Pty Ltd, Bankstown, Library
BHP, Melbourne Research Laboratories

SPARES (4 COPIES)

TOTAL (60 COPIES)

AL 149 DEPARTMENT OF DEFENCE

DOCUMENT CONTROL DATA

PAGE CLASSIFICATION: UNCLASSIFIED

PRIVACY MARKING:

1a. AR NUMBER	1b. ESTABLISHMENT NUMBER	2. DOCUMENT DATE	3. TASK NUMBER
AR-007-102	ARL-TR-10	NOVEMBER 1993	DST 92/128

4. TITLE

COMPUTATION OF NON-ISENTROPIC INTERNAL FLOWS WITH VARIABLE DENSITY

5. SECURITY CLASSIFICATION (PLACE APPROPRIATE CLASSIFICATION IN BOX(S) IE. SECRET (S), CONF. (C) RESTRICTED (R), LIMITED (L), UNCLASSIFIED (U)).

DOCUMENT	TITLE	ABSTRACT
U	U	U

6. NO. PAGES: 46

7. NO. REFS.: 8

8. AUTHOR(S)

E. BRIZUELA

9. DOWNGRADING/DELIMITING INSTRUCTIONS

Not applicable.

10. CORPORATE AUTHOR AND ADDRESS

AERONAUTICAL RESEARCH LABORATORY

AIRFRAMES AND ENGINES DIVISION

506 LORIMER STREET

FISHERMENS BEND VIC 3207

11. OFFICE/POSITION RESPONSIBLE FOR:

SPONSOR: DSTO

SECURITY: -

DOWNGRADING: -

APPROVAL: CAED

12. SECONDARY DISTRIBUTION (OF THIS DOCUMENT)

Approved for public release.

OVERSEAS ENQUIRIES OUTSIDE STATED LIMITATIONS SHOULD BE REFERRED THROUGH DSTIC, ADMINISTRATIVE SERVICES BRANCH, DEPARTMENT OF DEFENCE, ANZAC PARK WEST OFFICES, ACT 2601

13a. THIS DOCUMENT MAY BE ANNOUNCED IN CATALOGUES AND AWARENESS SERVICES AVAILABLE TO ....

No limitations.

13b. CITATION FOR OTHER PURPOSES (IE. CASUAL ANNOUNCEMENT) MAY BE [X] UNRESTRICTED OR [ ] AS FOR 13a.

14. DESCRIPTORS

Computational fluid dynamics
Numerical simulation
Gas turbine engines
Combustion chambers
Computer codes
Algorithms

15. DISCAT SUBJECT CATEGORIES

1201
2105

16. ABSTRACT

A computational fluid dynamics code named MULTIFLOW-2D has been acquired and is being put into service for the numerical simulation of gas turbine-type combustors.

Certain areas of the code were found to be in need of improvement for this application; these are:

- *The grid generation algorithm*
- *The manner of discretisation of the continuity and momentum equations, and*
- *The treatment of the inlet boundary conditions.*

PAGE CLASSIFICATION
UNCLASSIFIED
PRIVACY MARKING

THIS PAGE IS TO BE USED TO RECORD INFORMATION WHICH IS REQUIRED BY THE ESTABLISHMENT FOR ITS OWN USE BUT WHICH WILL NOT BE ADDED TO THE DISTR DATA UNLESS SPECIFICALLY REQUESTED.

16. ABSTRACT (CONT).

Improvements to these areas were developed and incorporated to the code, and the code functioning in non-reactive flows was tested by means of numerical experiments; verification against physical experiments is planned.

17. IMPRINT

AERONAUTICAL RESEARCH LABORATORY, MELBOURNE

18. DOCUMENT SERIES AND NUMBER	19. WA NUMBER	20. TYPE OF REPORT AND PERIOD COVERED
Technical Report 10	42 434F	

21. COMPUTER PROGRAMS USED

22. ESTABLISHMENT FILE REF.(S)

23. ADDITIONAL INFORMATION (AS REQUIRED)